International Journal of Mass Spectrometry 330–332 (2012) 285–294

Contents lists available at SciVerse ScienceDirect

International Journal of Mass Spectrometry

journal homepage: www.elsevier.com/locate/ijms

# On the path to glycan conformer identification: Gas-phase study of the anomers of methyl glycosides of *N*-acetyl-D-glucosamine and *N*-acetyl-D-galactosamine

Cesar S. Contreras[a,1], Nicolas C. Polfer[a], Jos Oomens[b,c,d], Jeffrey D. Steill[b,2], Brad Bendiak[e], John R. Eyler[a,*]

[a] Department of Chemistry, P.O. Box 117200, University of Florida, Gainesville, FL 32611-7200, USA
[b] FOM Institute for Plasma Physics Rijnhuizen, P.O. Box 1207, NL-3430 BE Nieuwegein, The Netherlands
[c] University of Amsterdam, Science Park 904, 1098XH Amsterdam, The Netherlands
[d] Radboud University Nijmegen, Institute for Molecules and Materials, Heyendaalseweg 135, 6525AJ Nijmegen, The Netherlands
[e] Department of Cell and Developmental Biology and Program in Structural Biology and Biophysics, University of Colorado Health Sciences Center, Denver, CO, USA

ARTICLE INFO

*Article history:*
Received 23 August 2012
Received in revised form
20 September 2012
Accepted 24 September 2012
Available online 4 October 2012

*Keywords:*
Monosaccharides
Mass spectrometry
Stereochemistry
Infrared photodissociation
Free-electron laser
*N*-acetyl group

ABSTRACT

The methyl glycosides of *N*-acetyl-D-glucosamine (D-GlcNAc) and *N*-acetyl-D-galactosamine (D-GalNAc) have been used as model glycan analogs to study the effects of lithium cation binding on glycan structure in gas-phase experiments. Infrared multiple photon dissociation (IRMPD) spectra for the two $Li^+$-complexed anomers of methyl-D-GlcNAc revealed a difference of 10 $cm^{-1}$ between their respective carbonyl stretching band positions. A corresponding 11 $cm^{-1}$ shift was observed for the two $Li^+$-complexed anomers of methyl-D-GalNAc. Theoretical calculations indicate that the position of the methyl group (α and β, or axial and equatorial, respectively) on carbon 1 of the sugar and its close proximity to the carbonyl of the acetamido group on carbon 2 cause the average orientation of the carbonyl to change in order to minimize steric hindrance. This change in orientation is postulated to be the cause of the observed C=O stretching band shift. The calculations also predict competitive binding of the lithium cation between two or more regions of D-GlcNAc and D-GalNAc. This is primarily due to differences in the spatial arrangement and orientation of lone pairs of electrons among the isomers, and stereochemical differences in hydrogen bonding. From an application point of view, differences in the infrared spectra of lithium adducts of acetamido sugars establish the value of variable-wavelength IRMPD as an alternative to fragmentation patterns in discriminating between these isomers.



## 1. Introduction

Gas-phase experiments with charged proteins and other large biomolecules continue to expand into new areas of interest in chemistry and biology as mass spectrometric techniques evolve to allow routine study of these large systems [1–7]. Fourier transform ion cyclotron resonance mass spectrometry (FTICR-MS) experiments [8–12], when combined with gentle ionization techniques such as electrospray ionization (ESI) [4,13–15] have the capability of studying sugar complexes without requiring heating of the sample (and thus inducing its possible decomposition) in order to introduce them into the gas phase. In FTICR-MS experiments sugars can be studied at low pressures (below $10^{-9}$ Torr), providing a virtually collision-free environment to investigate basic chemical processes. Collision induced dissociation (CID) [16] and single-frequency infrared multiple photon dissociation (IRMPD) methods have been used to study carbohydrate isomers in tandem MS experiments, both in the negative and positive ion modes [11,17–24]. In some cases, when either of these methods is used to examine isomeric compounds, particularly stereoisomers, differentiation of ions can be difficult as they yield near-identical dissociation patterns. Varying the wavelength of irradiation in IRMPD provides an extra dimension to analysis, in the expectation that stereoisomers may not absorb photons identically over a range of wavelengths [25–27]. Recent studies, using FTICR-MS in conjunction with variable wavelength IRMPD, have shed new light on the structures of carbohydrates [28–35]. Carbohydrates, even simple monosaccharides, can assume multiple configurations and/or conformations, sometimes favoring one over another depending on environmental influences such as interaction with different solvents, metals, and intramolecular hydrogen bonding [36–40]. A number of physical techniques, including crystallography [41], NMR [37], electrophoresis [42,43], mass spectrometry and theoretical calculations [40,44] have focused on

* Corresponding author. Tel.: +1 352 392 0532; fax: +1 352 392 0872.
*E-mail addresses:* cesar.contreras@nasa.gov (C.S. Contreras), polfer@chem.ufl.edu (N.C. Polfer), J.oomens@rijnhuizen.nl (J. Oomens), jdsteil@sandia.gov (J.D. Steill), Brad.Bendiak@UCDenver.edu (B. Bendiak), eylerjr@chem.ufl.edu (J.R. Eyler).
[1] Present address: NASA Ames Research Center, Moffett Field, CA, USA.
[2] Present address: Sandia/California, Livermore, CA, USA.

1387-3806/$ – see front matter © 2012 Elsevier B.V. All rights reserved.
http://dx.doi.org/10.1016/j.ijms.2012.09.010

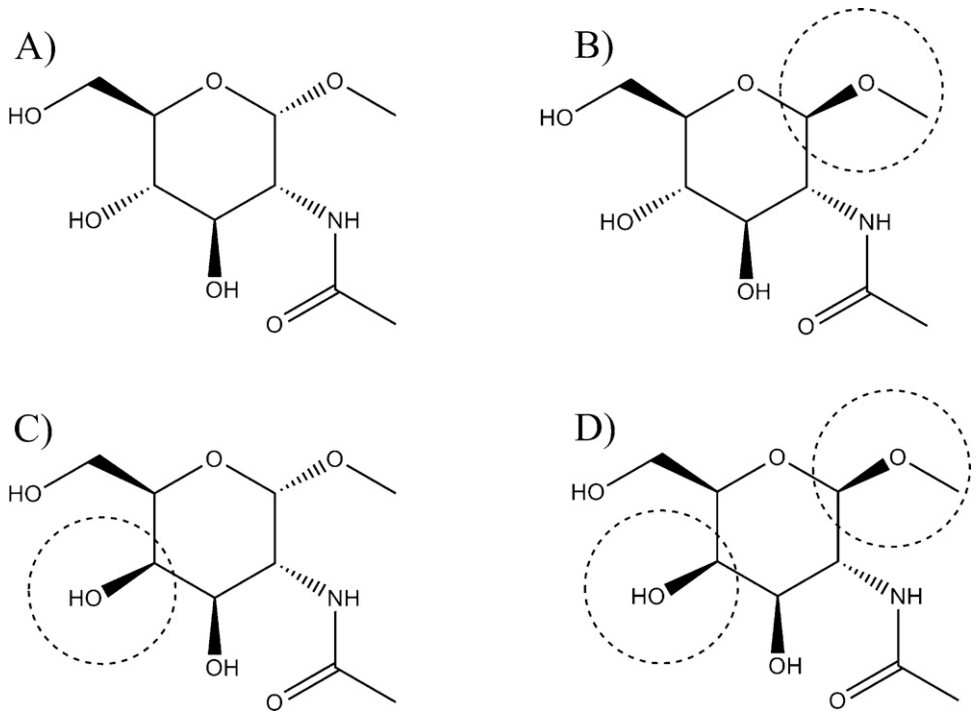


**Fig. 1.** Isomers α-methyl-D-GlcNAc (A), β-methyl-D-GlcNAc (B), α-methyl-D-GalNAc (C) and β-methyl-D-GalNAc (D). The differences between the α and β anomers at carbon 1 and epimers of glucose and galactose at carbon 4 are shown encircled in dashed outlines.

the interactions of metal ions with sugars. The conformation of glycans affects their role as components of larger biomolecules; they are important in cell–cell signaling [45] and have been found to affect protein folding [46], often stabilizing the protein structure.

To obtain a more complete picture of the role of oligosaccharides in protein-based systems, the interactions between alkali metals and sugars need to be understood in greater detail. Sodium and potassium play a crucial role in regulating cell functions and their blood concentration levels are carefully regulated in biological systems. Lithium ions are used as strong prescription drugs to regulate mood. Practically, alkali metals more readily adduct with sugars and such charged adducts can be transferred to the gas phase using electrospray ionization. This provides adequate abundances of precursor ions required to conduct reliable MS/MS experiments. If the alkali cation–sugar interaction is strong, fragmentation pathways other than simple cation loss may be favored when ions are subjected to irradiation with an infrared laser or CID. Intramolecular fragmentation is usually observed for $Li^+$-complexed saccharides [17,47]. In the present work fragmentation of stereoisomers, specifically the methyl glycosides of α- and β-*N*-acetyl-D-glucosamine (α-methyl-D-GlcNAc and β-methyl-D-GlcNAc) and α- and β-*N*-acetyl-D-galactosamine (α-methyl-D-GalNAc and β-methyl-D-GalNAc) (Fig. 1) bound to a lithium cation was studied as a function of infrared laser irradiation wavelength. The infrared multiple photon dissociation (IRMPD) spectra obtained, as well as differences in fragmentation patterns for the complexes, are combined with theoretical calculations of ion structures and simulated spectra to provide important information about their gas-phase structures.

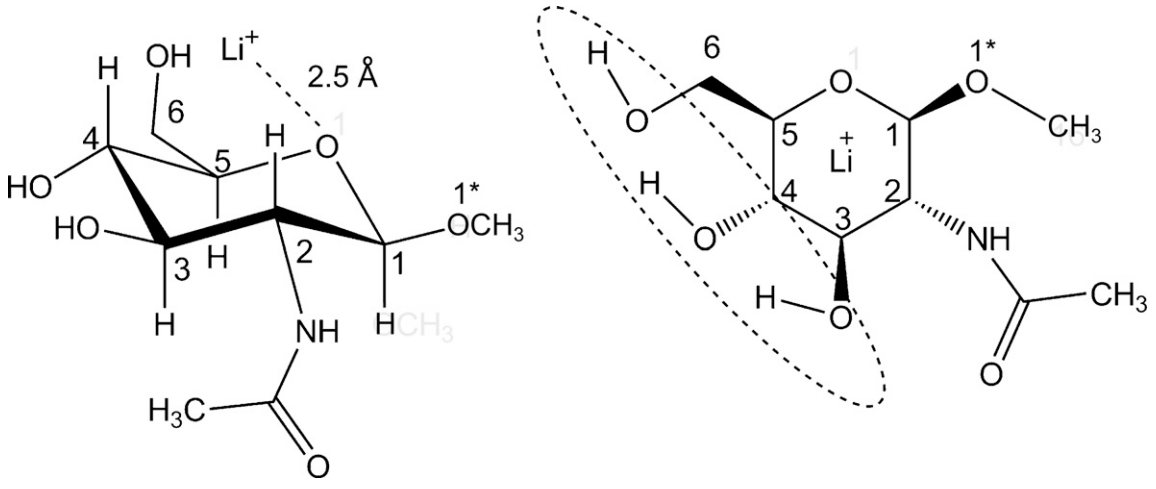


**Fig. 2.** Side (left) and top (right) views of β-methyl-D-GlcNAc. Lithium was initially placed above the ring, approximately 2.5 Å from the ring oxygen. The clockwise hydrogen-bonding network is visible in the top view and is encircled in a dashed outline. The carbons are numbered 1–6, and 1* marks the glycosidic oxygen of the O-methyl group bonded to the anomeric carbon (C-1).

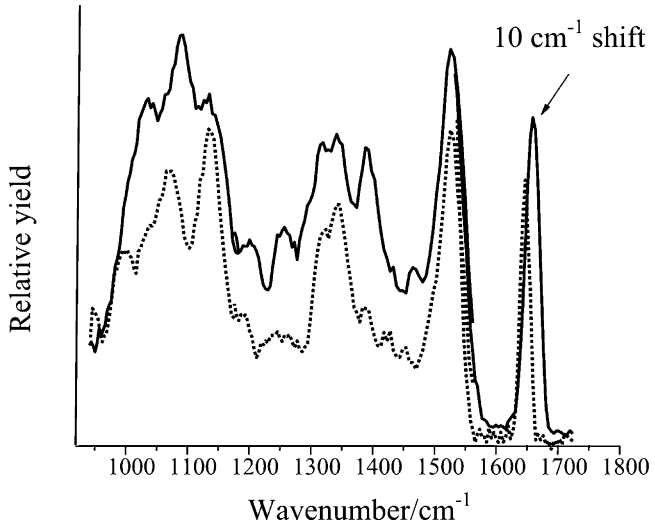


**Fig. 3.** IRPMD spectra of α-methyl-D-GlcNAc (dashed line) and β-methyl-D-GlcNAc (solid line) bound to a lithium cation, showing the 10 $cm^{-1}$ red shift of the carbonyl stretching frequency for the α anomer.

## 2. Materials and methods

### 2.1. Sample preparation

The methyl glycosides of α- and β-D-GlcNAc were obtained from Sigma Chemical Co. (St. Louis, MO) and α- and β-D-GalNAc were purchased from Behring Diagnostics (Calbiochem, La Jolla, CA). Stock solutions were made by dissolving 0.01 mg/mL of the respective glycoside in 80:20 $CH_3OH$:$H_2O$ solution. Stock samples were diluted by a factor of 10 and were mixed with an equimolar amount of LiCl before introduction into the electrospray ionization source.

### 2.2. Instrumentation

All ESI-FTICR-MS experiments were carried out using a laboratory-built FTICR mass spectrometer equipped with a 4.7 T superconducting magnet (Cryomagnetics Inc., Oak Ridge, TN), which has been described previously [28,48,49]. An external Z-spray source (Micromass/Waters Corporation, Milford, MA) injects the samples into the ESI source at a flow rate of 10 μL/min. Electrospray ionization efficiency was aided with a nebulizer and a desolvation gas, both $N_2$ gas, with a continuous flow of 35 and 155 l/h, respectively. Source temperature was set to 52 °C and the desolvation gas temperature was 125 °C. The electrospray needle-sampling cone voltage difference was set to 3 kV. Precursor ions were isolated using stored waveform inverse Fourier transform (SWIFT) waveforms [50,51] to eject all other ions. Ions were detected using the broadband detection mode covering a mass range from 20 to 2000 Da.

The fragmentation of the lithiated HexNAc methyl glycosides as a function of laser irradiation wavelength provides the IRMPD spectra. These gas phase infrared spectra can be compared with theoretical calculations of the vibrational frequencies to obtain band assignments and structural information for each isomer. For the IRMPD activation, a free electron laser located at the FOM Institute for Plasma Physics Rijnhuizen, in Nieuwegein, The Netherlands [52], was used to scan the infrared fingerprint region from 900 to 1800 $cm^{-1}$ for the methyl-GlcNAc anomers. Since the desired spectral feature was the shift of the carbonyl stretching frequency for the methyl-GalNAc anomers, the spectra were taken only from 1400 to 1700 $cm^{-1}$. Four individual transients were accumulated at each wavelength to improve the signal-to-noise ratio. Three independent IRMPD spectra were used to calculate the average peak position of the C=O stretch band for each isomer. The IRMPD yield at a given frequency is calculated from the measured intensities of the precursor and product ions, $I_{prec}$ and $I_{prod}$, respectively, corrected for the frequency-dependent laser power $P(\omega)$.

$$\text{Relative IRMPD yield} = (P(\omega))^{-1} \times \ln\left[\frac{\sum I_{prod}}{I_{prec} + \sum I_{prod}}\right]$$

## 3. Theory/calculation

Molecular mechanics conformational searches using the AMBER force field [53] were conducted and density functional theory (DFT) [54–56] geometry optimizations and frequency calculations were used to identify spectral features of each methyl-HexNAc isomer. Using the structure database provided in the Hyperchem software [57], each anomer of methyl-D-GlcNAc and methyl-D-GalNAc was examined as a clockwise hydrogen bonding network, which has been shown to be the most stable solution-phase structure for D-glucopyranosides [58–60]. Lithium was initially placed centered above the ring system of the glycan, approximately 2.5 Å from the ring oxygen (Fig. 2). Each methyl-HexNAc adduct was given an overall charge of +1.

A conformational search of torsion angles was done to probe the rearrangement of each isomer during its interaction with the lithium cation. All calculations were performed in an isolated

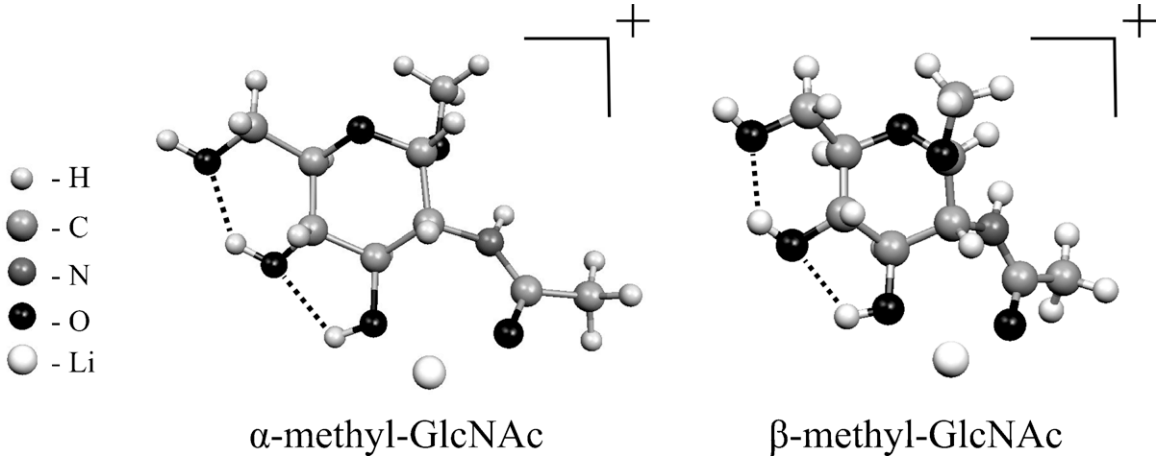


**Fig. 4.** Calculated lowest energy structures of α-methyl-GlcNAc and β-methyl-GlcNAc, using B3LYP/6-311++G(d,p), with hydrogen bonds shown as dotted lines.

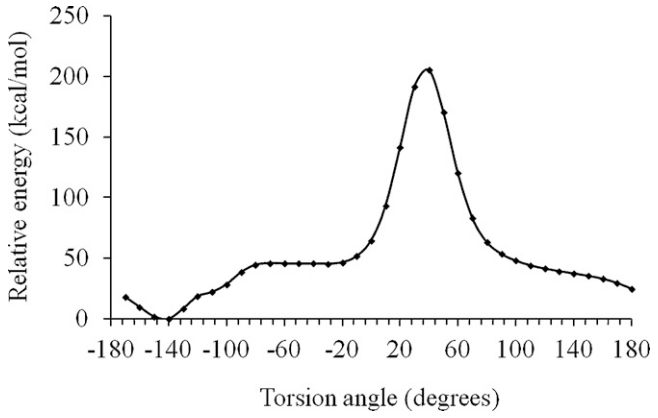


**Fig. 5.** Potential surface scan for rotation about the (C-2)—N bond for α-methyl-GlcNAc.

environment. All H—C—O—H torsion angles were defined so that the O—H functional group could rotate about the C—O bonds, thus keeping the structural definitions for each HexNAc intact. The ring torsion angles were varied in the conformational search, making sure that the orientation of chiral centers did not change. Using the usage-directed approach [61], 1000 different structures were created with the algorithm. For each step, the dihedral angles were randomly changed to create a new structure, and a geometry optimization using the AMBER force field [53] was performed to verify a stable point. The optimized structure was compared to the other stable structures previously obtained from the conformational search, and duplicate structures were discarded. On average, the 100 most stable structures within 15 kcal/mol of the structure having the lowest energy were subsequently geometry optimized using Gaussian 03 [62] with the B3LYP/6-311++G(d,p) level of theory. A frequency calculation at this same level of theory was conducted for each structure to verify energy minima and to compare the resulting theoretical infrared spectra to experimental spectra. This level of theory has been used previously to study sugars in the gas phase [63–65]. A scaling factor of 0.98 was used for the calculated frequencies, and is within the range of reported average scaling factors using this basis set [66–68]. For further verification that the lowest energy conformer was found for each stereoisomer, a rigid potential surface scan of the H—(C-2)—N—H dihedral angle was carried out using Gaussian 03 with B3LYP/6-311++G(d,p). Single point calculations were performed as the amide hydrogen atom was rotated by 10° increments about the (C-2)—N sigma bond, while keeping the rest of the molecule fixed.

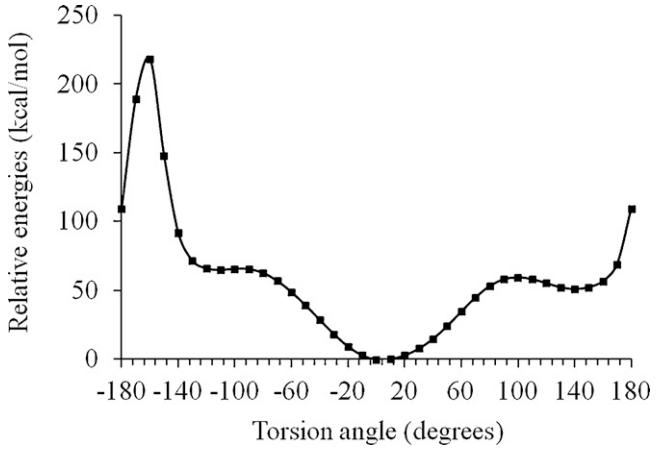


**Fig. 6.** Potential surface scan for rotation about the (C-2)—N bond for β-methyl-GlcNAc.

**Table 1**
Relative energies of methyl-HexNAc isomer structures obtained from the corresponding conformational searches. Relative energies were obtained at the B3LYP/6-311++G(d,p) level of theory and are given in kcal/mol. Conformer 1 of each isomer is shown in Fig. 4 (methyl-GlcNAc anomers) and Fig. 10 (methyl-GalNAc anomers).

| Conformer # | α-Me-GlcNAc | β-Me-GlcNAc | α-Me-GalNAc | β-Me-GalNAc |
|---|---|---|---|---|
| 1 | 0.0 | 0.0 | 0.0 | 0.0 |
| 2 | 2.2 | 0.2 | 4.2 | 1.9 |
| 3 | 5.3 | 10.5 | 4.2 | 2.5 |
| 4 | 7.5 | 12.1 | 4.7 | 2.5 |
| 5 | 9.2 | 13.4 | 4.7 | 3.0 |
| 6 | 10.2 | 14.8 | 5.9 | 3.4 |
| 7 | 12.1 | 15.1 | 7.6 | 3.5 |
| 8 | 12.2 | 15.3 | 8.3 | 4.7 |
| 9 | 14.9 | 18.1 | 8.3 | 4.9 |
| 10 | 19.6 | 20.1 | 8.6 | 6.0 |

Structures with an initial boat configuration of the ring were also investigated and optimized at the same level of theory as those that started with a chair configuration of the ring. Optimizations were conducted for different starting positions of the lithium cation around the ring system. All optimized structures were compared to obtain the lowest energy conformers.

## 4. Results and discussion

### 4.1. α- and β-methyl-N-acetyl-D-glucosamines

#### 4.1.1. Experimental infrared multiple photon dissociation spectra

The experimental IRMPD spectra of the methyl glycosides of both α- and β-GlcNAc are shown in Fig. 3. The spectral bands in the range from 800 to 1500 $cm^{-1}$ are broad and, although there are differences at some wavelengths between the spectra of the two anomers, such as near 1100, 1250 and 1380 $cm^{-1}$, definitive spectral assignments are not feasible in this region. However, when comparing the spectra of the two anomers, a shift in the position of the band near 1652 $cm^{-1}$ was clearly seen. Repeating the IRMPD spectra 3 times, an average red shift of 10 $cm^{-1}$ was observed for the α anomer.

#### 4.1.2. Calculations of minimal energy structures

The calculated lowest energy structures for α-methyl-GlcNAc and β-methyl-GlcNAc, each coordinated with a lithium ion, are shown in Fig. 4. The α-methyl-D-GlcNAc anomer has a chair $^4C_1$ conformation, with evident hydrogen bonding, while

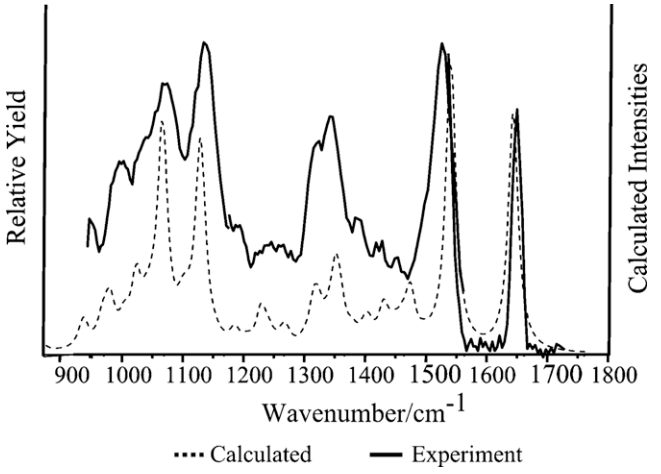


**Fig. 7.** Comparison of experimental IRMPD and calculated infrared spectra for α-methyl-GlcNAc. The calculated spectrum has been scaled by 0.98, and has a 20 $cm^{-1}$ Gaussian band profile.

β-methyl-D-GlcNAc's lowest energy conformer has a $B_{O3}$ boat conformation. For both α- and β-methyl-GlcNAc, two hydrogen bonds are formed among the hydroxyl groups OH-3, OH-4 and OH-6.

With the methyl group at C-1 in the axial position, α-methyl-GlcNAc has the amide hydrogen located nearest to the glycosidic oxygen. To minimize steric hindrance, the carbonyl is oriented away from the O-methyl group. A rigid potential surface scan of the dihedral angle rotation about the (C-2)—N bond led to one stable minimum, with one other possible stationary point at ~-30° along the potential energy surface (Fig. 5). The lowest energy conformation revealed the lithium ion interacting with both the carbonyl of the acetamido group and the oxygen of OH-3. The point of highest energy corresponds to the structure in which the carbonyl oxygen is in close contact with the O-methyl group.

For the lowest energy structure of β-methyl-GlcNAc, the methyl group is nearly in the axial position for a skewed boat conformer (Fig. 4). The acetamido group is oriented so that the oxygen interacts with the lithium cation. The potential surface scan, shown in Fig. 6, indicates that the torsion angle of 3° for the H—(C-2)—N—H dihedral corresponds to the lowest energy structure in the range of 0–360°. The highest energy position of the dihedral occurs when the *N*-acetyl methyl group is closest to the lithium cation, which is located between the *N*-acetyl and the C-3 hydroxyl group. Two other minima were found in the dihedral scan, with potential energy barriers of 60 and 66 kcal/mol between the minima.

Based on the calculated structures, the observed α vs. β anomer frequency shifts for the carbonyl stretching band apparently result from a complex interplay between the partial charge on the lithium cation (0.58 for the β anomer, 0.66 for the α anomer), and the O-3 – $Li^+$-carbonyl oxygen bonding angle. Also, one other structure where the lithium cation was located at a different position around β-methyl-GlcNAc was higher in energy by only 0.2 kcal/mol, as shown in Table 1. That structure (#2 in the table) has a chair conformation and the lithium is located near the oxygen of the ring system. Given that a substantial portion of the $Li^+$-β-methyl-GlcNAc ions probably have this structure, the fact that the lithium cation is relatively far from the C=O bond would keep the carbonyl stretching frequency from being significantly red shifted. Structure #2 will also be included in the analysis of β-GlcNAc, when comparing the calculated infrared spectra to the experimental results.

### 4.1.3. Theoretical spectra

Calculations of infrared spectra indicate that the band near 1652 $cm^{-1}$ is the C=O stretch of the carbonyl on the acetamido (—$NHCO(CH_3)$) group. There was a corresponding shift of 9.8 $cm^{-1}$ between the calculated frequencies of this band for the two anomers of methyl-GlcNAc using the B3LYP/6-311++G(d,p) level of theory for the vibration frequencies [66,67].

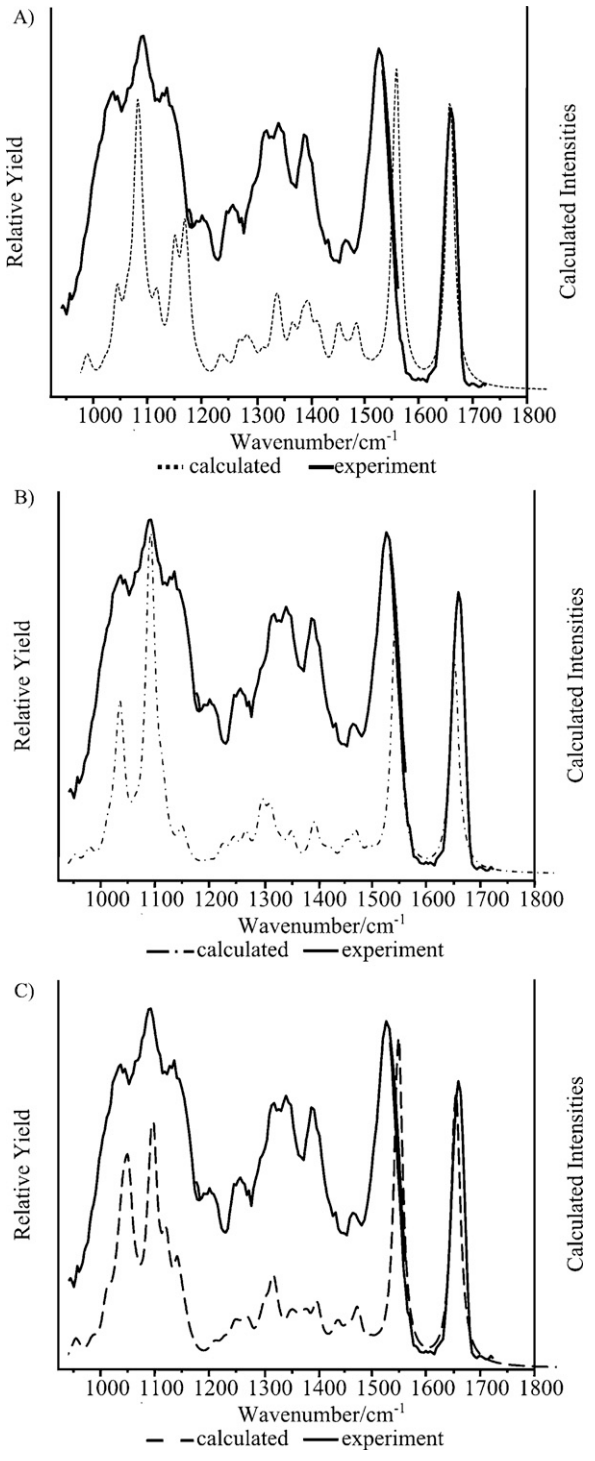


**Fig. 8.** Comparison of experimental IRMPD spectrum (solid line) to the calculated infrared spectrum (dashed line) of β-methyl-GlcNAc from (A) the lowest energy conformer, (B) the next lowest energy conformer (0.2 kcal/mol higher is energy) and (C) a composite spectrum calculated from a weighted Boltzmann contribution of each conformer.

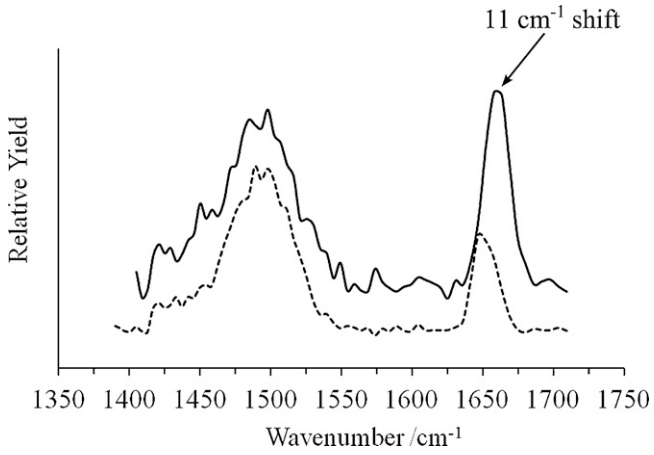


**Fig. 9.** IRMPD spectra of α-methyl-GalNAc (dashed line) and β-methyl-GalNAc (solid line), showing an 11 $cm^{-1}$ difference for the position of the carbonyl stretch bands.

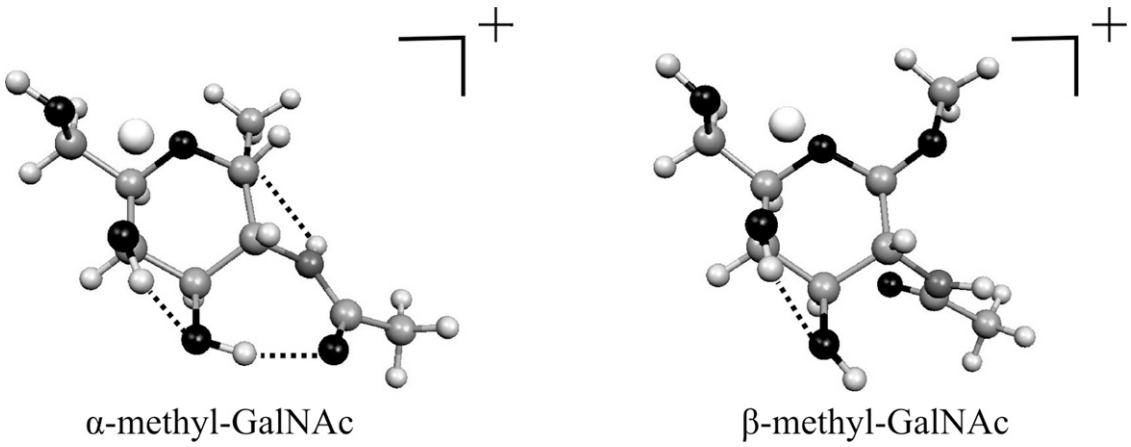


**Fig. 10.** Lowest energy structures of the anomers of methyl-D-GalNAc from B3LYP/6-311++G(d,p) calculations, with hydrogen bonds shown as dotted lines.

The calculated spectrum of the lowest energy structure for α-methyl-GlcNAc is similar to the experimental spectrum, having similar partially unresolved features between 800 and 1500 $cm^{-1}$ (Fig. 7). The calculated C=O stretch frequency after scaling is 1632 $cm^{-1}$.

The calculated spectra of the two lowest energy structures for β-methyl-GlcNAc are shown in Fig. 8. Again, there are many absorbtion bands in the calculated spectrum from 800 to 1500 $cm^{-1}$, although they matched the experimental spectrum in this region less well than those of the α anomer (Fig. 7). The calculated C=O stretch after scaling is 1642 $cm^{-1}$ for β-methyl-GlcNAc, higher by 10 $cm^{-1}$ than that for the α anomer and in agreement with the experimental wavenumber shift. A weighted average spectrum based on spectra of the two lowest energy β-methyl-GlcNAc structures was calculated from a Boltzmann probability ($P$) distribution of the two conformers:

$$P = \frac{\exp[-(\Delta E/RT)]}{\sum_j(\exp[-(\Delta E_j/RT)])},$$

where $\Delta E_j$ is the energy of the $j$th conformer relative to the lowest energy conformer, $R$ is the Boltzmann constant and $T$ is the temperature, chosen as 298.15 K. The composite spectrum intensities ($I_C$) were then calculated as the sum of the original theoretical intensities of structures 1 ($I_1$) and 2 ($I_2$) multiplied by their respective Boltzmann factors, $I_C = I_1 \times P_1 + I_2 \times P_2$.

### 4.2. α- and β-methyl-N-acetyl-D-galactosamines

#### 4.2.1. Experimental infrared multiple photon dissociation spectra

Following analysis of the methyl glycosides of *N*-acetylglucosamine, where the major assignable feature in the IRMPD spectra was the carbonyl stretch, spectra for the anomers of methyl-D-GalNAc were only taken from 1400 to 1700 $cm^{-1}$ and are shown in Fig. 9. An 11 $cm^{-1}$ shift in band position was observed between α-methyl-GalNAc and β-methyl-GalNAc, with the band for the α-anomer lower than that for the β-anomer, as was also seen for the GlcNAc anomers.

#### 4.2.2. Calculations of minimal energy structures

The lowest energy structures from the DFT calculations are shown in Fig. 10, and have the $^4C_1$ ring conformation. Examination of the α-methyl-GalNAc structure reveals hydrogen bonding between the C-3 and C-4 hydroxyl groups, and between the carbonyl oxygen and the hydroxyl group at C-3. Other potential hydrogen bonds are interrupted due to coordination of the lithium cation to the oxygen lone pairs of —OH 4 and —OH 6. There is also a hydrogen bond between the amide hydrogen and the glycosidic oxygen.

β-Methyl-GalNAc (Fig. 10) has one hydrogen bond between the C-3 and C-4 OH groups. For the GlcNAc anomers, lithium was predicted to be located between the amide oxygen and the OH-3 group, but for the GalNAc anomers there is a tridentate interaction of the lithium and the O-4, O-5 and O-6 electron lone pairs. Thus the carbonyl stretching frequency shift observed for the GalNAc anomers is due to a different set of interactions. Most important in this case

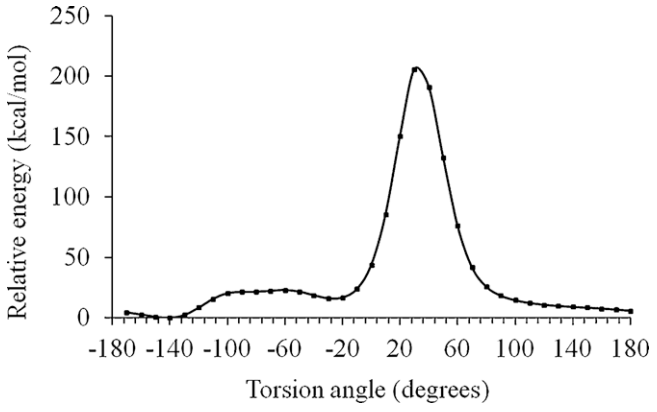


**Fig. 11.** Potential surface scan for rotation about the (C-2)—N bond for α-methyl-GalNAc.

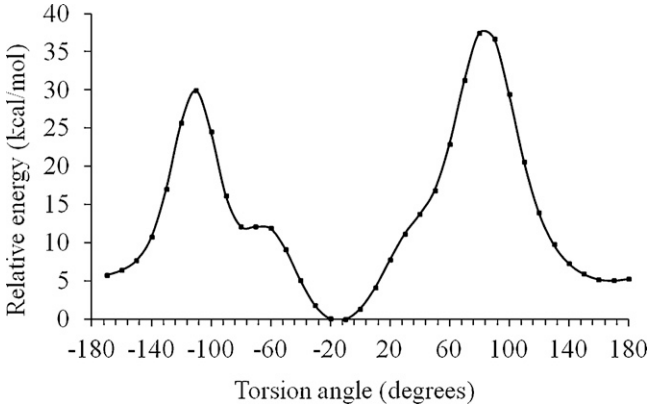


**Fig. 12.** Potential surface scan for rotation about the (C-2)—N bond for β-methyl-GalNAc.

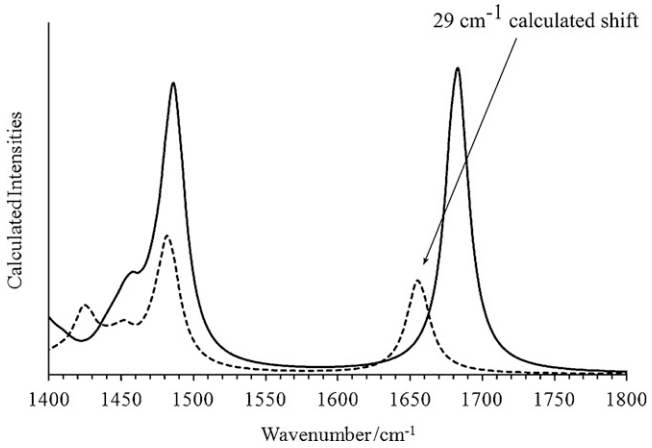


**Fig. 13.** Calculated infrared spectra of α-methyl-GalNAc (dashed line) and β-methyl-GalNAc (solid line), indicating a 29 $cm^{-1}$ shift in the C=O stretching frequencies.

is the direct hydrogen bonding of the carbonyl to —OH-3 for the α anomer, which would shift the carbonyl stretch band frequency to a lower value (as seen experimentally).

The potential surface scans of α- and β-methyl-GalNAc (torsion about the (C-2)—N bond) indicate that the conformers found in the conformational search and used throughout this analysis are the lowest points on the 1-dimensional surface (Figs. 11 and 12).

The highest energy points on these surfaces correspond to structures in which the carbonyl oxygen is in close proximity to the O-methyl oxygen at C-1 for both anomers of methyl-D-GalNAc and these structures are analogous to those corresponding to the highest energy points on the potential surface scans for the D-GlcNAc anomers. The α-methyl-GalNAc lithium cation is bound to the ring oxygen and the oxygens of —OH 4 and 6, and has a charge of 0.57. The interactions of the lithium cation with the oxygens of β-methyl-GalNAc are the same as those of the α-anomer (the ring oxygen and those of —OH 4 and 6), with a correspondingly similar charge of 0.58 on the lithium cation. The charge on the lithium cation is higher for the methyl-GlcNAc anomers than for the methyl-GalNAc anomers as is evident from the interactions just reported. This may in part be due to the different stereochemistry at the 4-position which enables the 4-hydroxy oxygen to participate in a unique tridentate coordination complex with lithium, which is not possible with either anomer of the methyl glycosides of GlcNAc. A table of the relative energies using DFT for the 10 lowest energy forms of the HexNAc methyl glycoside structures from the conformational search is given above (Table 1).

#### 4.2.3. Theoretical spectra

The calculated spectra indicate a shift of 29 $cm^{-1}$ for the C=O stretch frequencies (Fig. 13). This is larger than the 11 $cm^{-1}$ shift observed experimentally for the Me-GalNAc anomers, and also larger than that seen and predicted theoretically for the Me-GlcNAc anomers. However, the band for the α anomer is always predicted

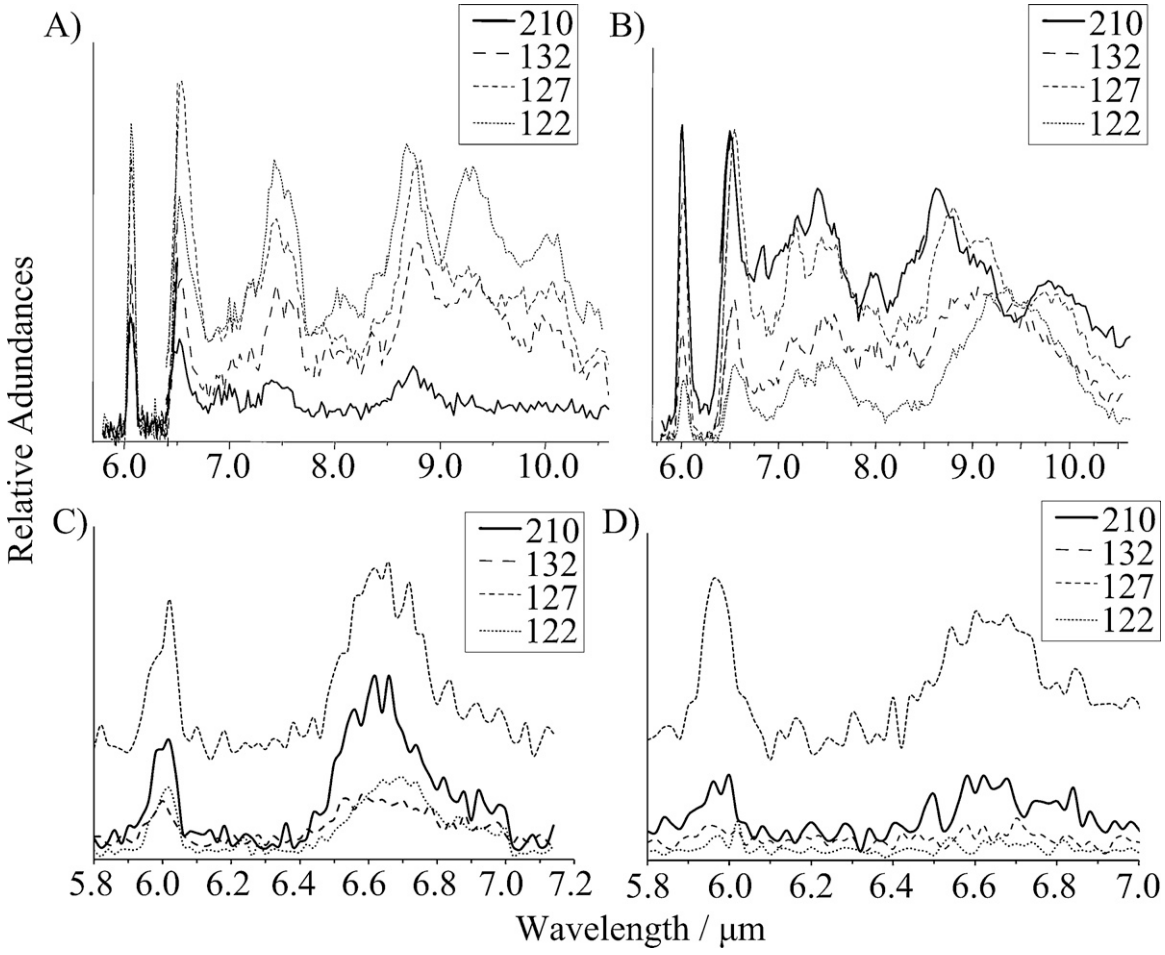


**Fig. 14.** Fragment ion abundances as a function of laser wavelength for the four methyl-HexNAc stereoisomers: (A) α-methyl-GlcNAc, (B) β-methyl-GlcNAc, (C) α-methyl-GalNAc, and (D) β-methyl-GalNAc.

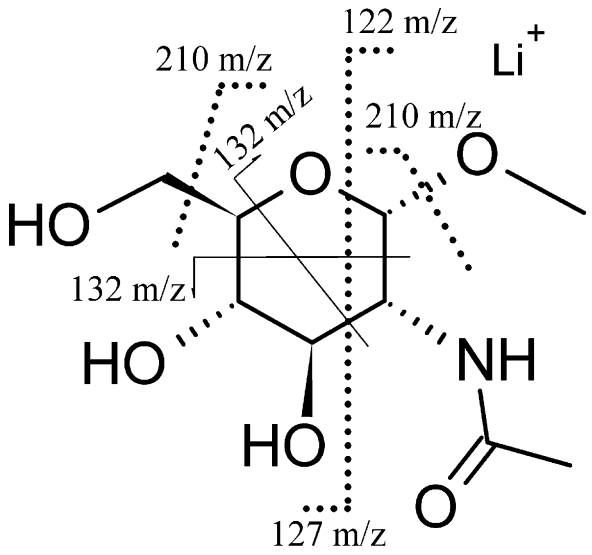


**Fig. 15.** Possible fragmentation patterns of methyl-HexNAc stereoisomers leading to spectra seen in Fig. 14. Black dotted lines indicate fragment ions to which a lithium cation is adducted and solid lines with an arrow indicate fragment ions without the lithium cation.

to be red-shifted compared to that for the β anomer as observed experimentally.

### 4.3. Fragmentation patterns

In the tandem mass spectra produced by IRMPD fragmentation of all four stereoisomers, four fragments were produced for each of the sugars (Fig. 14). One fragmentation channel involves the neutral loss of methanol ($CH_3OH$) (210 *m/z*), either from the aglycon or from position 6 of the precursor ion (242 *m/z*). Neutral losses may either be accompanied by desaturation of precursor ions (double bond formation) or through reactions that generate anhydrosugar products; both types of mechanisms occur in thermal degradation of neutral sugars and glycosides [69]. A larger fragment (127 *m/z*) is produced by cross-ring cleavage at C-1—O1 and C-2—C-3, resulting in a 4-carbon product ion originating from carbons C-3 to C-6, possibly a lithiated aldotetrose, with a neutral loss of 115 Da containing the aglycon, carbons C-1 and C-2, as well as the acetamido group. Another product ion (122 m/z) may represent the same structure as the 115 Da neutral loss, but now adducted to lithium (115 + 7 = 122 *m/z*), with a neutral loss of 120 Da, possibly similar in structure to the *m/z* 127 ion, but without the adducted lithium (127 – 7 = 120 Da). The *m/z* 132 product ion(s) appear to be protonated, rather than lithiated product ions, with neutral loss of 110 Da comprising a fragment having $Li^+$ $alkoxy^-$ structure(s) derived by cross-ring cleavages indicated in Fig. 15. These dissociation sites are a working model and more information about their exact structures and possible isomeric composition would need to be derived from additional experiments.

However, it is noteworthy that significant, wavelength-dependent differences in product ion ratios were seen among the isomers that displayed a stereochemical dependence. For example, for the β-methyl-GlcNAc isomer, the *m/z* 210 product ion was the highest abundance product over much of the wavelength range studied, whereas it was of lowest abundance for the α-methyl-GlcNAc isomer and of second highest abundance over much of the wavelength range studied for the GalNAc isomers (Fig. 14). Similarly, the *m/z* 122 product ion was of greatest abundance over much of the wavelength range investigated for the α-methyl-GlcNAc isomer, yet was of lowest abundance over most of the wavelength range for the β-methyl-GlcNAc isomer and of quite low abundance for both GalNAc isomers. The *m/z* 127 product ion was most abundant for the methyl-GalNAc isomers. In addition to these more general differences in product ion ratios between isomers, there were unique differences in ratios observable for each isomer that were wavelength-dependent (i.e. where abundances of product ions crossed over as a function of wavelength or became significantly different in relative amounts, Fig. 14). These differences point out specific wavelengths where a judicious choice of laser power could be used to selectively dissociate and/or to differentiate them in the gas phase. As such, variable-wavelength infrared photodissociation may be used as an alternative, and more isomer-selective, tool for dissociation than collision-induced dissociation, where a wide range of energies are imparted to precursor ions.

## 5. Conclusions

Differentiation of HexNAc methyl glycosides in the gas phase with IRMPD spectra is possible because each isomer either has distinct infrared spectral features or fragmentation patterns in the tandem mass spectra. In this study C=O stretching mode band shifts (10 and 11 $cm^{-1}$) were observed for the lithium cationized anomers of methyl-GlcNAc and methyl-GalNAc, respectively, and these can be used to differentiate the anomers. The shifts in C=O stretches between the α and β anomers are explained using theoretically calculated spectra as resulting from the difference in orientation of the acetamido carbonyl, which is influenced either by the binding location of a lithium ion between epimers of methyl-GlcNAc and methyl-GalNAc, and alternate hydrogen bonding of the acetamido group between OH-3 for the anomers of methyl-GlcNAc, as well as the glycosidic oxygen position for the anomers of methyl-GalNAc. The favorable interaction of the amide hydrogen with the O-methyl oxygen also influences the location of the carbonyl, since both are part of the acetamido group. Calculated structures indicate that the lithium cation is located between C-3 and the acetamido group for α/β-methyl-GlcNAc. In the calculated structures of α/β-methyl-GalNAc, the lithium cation is found to interact with 3 oxygens: the ring oxygen, and the 4- and 6-hydroxyl oxygens. Other defining spectral features, which could be seen in different IR wavelength ranges, can also be used to further differentiate the isomers.

From a purely analytical perspective, variation of the wavelength of infrared irradiation provides another dimension to analyses where differences in both the total ion abundance and abundances of each independent product ion are a function of laser wavelength. This enables optimal differentiation of isomers to be assessed over a reasonably broad wavelength range and may permit selective isomer dissociation to be achieved using isomeric mixtures in the future.

## Acknowledgments

The authors are grateful to the National Science Foundation for funding under Grants CHE-0718007 and OISE-0730072. This work is part of a research program of FOM, which is financially supported by the 'Nederlandse Organisatie voor Wetenschappelijk Onderzoek' (NWO). Assistance of the FELIX staff is greatly acknowledged. Construction and shipping of the FTICR mass spectrometer were supported with funding from the National High Magnetic Field Laboratory, Tallahassee, Florida (Grant CHE-9909502).

## References

[1] M. Dole, L.L. Mack, R.L. Hines, R.C. Mobley, L.D. Ferguson, M.B. Alice, Molecular beams of macroions, Journal of Chemical Physics 49 (1968) 2240–2249.
[2] K. Tanaka, Y. Ido, S. Akita, Y. Yoshida, T. Yoshida, Detection of high mass molecules by laser desorption mass spectrometry, Iyo Masu Kenkyukai Koenshu 12 (1987) 219–222.

[3] M. Karas, F. Hillenkamp, Laser desorption ionization of proteins with molecular masses exceeding 10,000 daltons, Analytical Chemistry 60 (1988) 2299–2301.
[4] J.B. Fenn, M. Mann, K. Meng, S.F. Wong, C.M. Whitehouse, Electrospray ionization for mass spectrometry of large biomolecules, Science 246 (1989) 64–71.
[5] J. Zaia, Mass spectrometry of oligosaccharides, Mass Spectrometry Reviews 23 (2004) 161–227.
[6] D. van den Boom, F. Hillenkamp, Analysis of nucleic acids by mass spectrometry, in: Analytical Techniques in DNA Sequencing, CRC Press, Boca Raton, FL, 2005, pp. 85-106.
[7] R.B. Cole (Ed.), Electrospray and MALDI Mass Spectrometry: Fundamentals, Instrumentation, Practicalities, and Biological Applications, second ed., John Wiley & Sons, Hoboken, NJ, 2010.
[8] A.G. Marshall, P.B. Grosshans, Fourier transform ion cyclotron resonance mass spectrometry – the teenage years, Analytical Chemistry 63 (1991) A215–A229.
[9] I.J. Amster, Fourier transform mass spectrometry, Journal of Mass Spectrometry 31 (1996) 1325–1337.
[10] A.G. Marshall, C.L. Hendrickson, G.S. Jackson, Fourier transform ion cyclotron resonance mass spectrometry: a primer, Mass Spectrometry Reviews 17 (1998) 1–35.
[11] Y. Park, C.B. Lebrilla, Application of Fourier transform ion cyclotron resonance mass spectrometry to oligosaccharides, Mass Spectrometry Reviews 24 (2005) 232–264.
[12] A.G. Marshall, C.L. Hendrickson, M.R. Emmett, R.P. Rodgers, G.T. Blakney, C.L. Nilsson, Fourier transform ion cyclotron resonance: state of the art, European Journal of Mass Spectrometry 13 (2007) 57–59.
[13] R.D. Smith, J.A. Loo, C.G. Edmonds, C.J. Barinaga, H.R. Udseth, New developments in biochemical mass spectrometry: electrospray ionization, Analytical Chemistry 62 (1990) 882–899.
[14] M. Mann, M. Wilm, Electrospray mass spectrometry for protein characterization, Trends in Biochemical Sciences 20 (1995) 219–224.
[15] R. Boyd, Electrospray ionization mass spectrometry: fundamentals, instrumentation, and applications, Journal of the American Society for Mass Spectrometry 8 (1997) 1191–1192.
[16] K.L. Busch, G.L. Glish, S.A. McLuckey, Mass Spectrometry/Mass Spectrometry: Techniques and Applications of Tandem Mass Spectrometry, VCH, New York, 1988.
[17] G.E. Hofmeister, Z. Zhou, J.A. Leary, Linkage position determination in lithium-cationized disaccharides – tandem mass spectrometry and semiempirical calculations, Journal of the American Chemical Society 113 (1991) 5964–5970.
[18] A. Fura, J.A. Leary, Differentiation of $Ca^{2+}$-coordinated and $Mg^{2+}$-coordinated branched trisaccharide isomers – an electrospray ionization and tandem mass spectrometry study, Analytical Chemistry 65 (1993) 2805–2811.
[19] S. Konig, J.A. Leary, Evidence for linkage position determination in cobalt coordinated pentasaccharides using ion trap mass spectrometry, Journal of the American Society for Mass Spectrometry 9 (1998) 1125–1134.
[20] J.Y. Salpin, J. Tortajada, Structural characterization of hexoses and pentoses using lead cationization. An electrospray ionization and tandem mass spectrometric study, Journal of Mass Spectrometry 37 (2002) 379–388.
[21] Y.J. Jiang, R.B. Cole, Oligosaccharide analysis using anion attachment in negative mode electrospray mass spectrometry, Journal of the American Society for Mass Spectrometry 16 (2005) 60–70.
[22] T.T. Fang, B. Bendiak, The stereochemical dependence of unimolecular dissociation of monosaccharide-glycolaldehyde anions in the gas phase: a basis for assignment of the stereochemistry and anomeric configuration of monosaccharides in oligosaccharides by mass spectrometry via a key discriminatory product ion of disaccharide fragmentation, $m/z$ 221, Journal of the American Chemical Society 129 (2007) 9721–9736.
[23] J.A. Rodrigues, A.M. Taylor, D.P. Sumpton, J.C. Reynolds, R. Pickford, J. Thomas-Oates, Mass spectrometry of carbohydrates: newer aspects, Advances in Carbohydrate Chemistry and Biochemistry 61 (2008) 59–141.
[24] B. Bendiak, T.T. Fang, Assignment of the stereochemistry and anomeric configuration of structurally informative product ions derived from disaccharides: infrared photodissociation of glycosyl-glycolaldehydes in the negative ion mode, Carbohydrate Research 345 (2010) 2390–2400.
[25] J.R. Eyler, Infrared multiple photon dissociation spectroscopy of ions in Penning traps, Mass Spectrometry Reviews 28 (2009) 448–467.
[26] N.C. Polfer, J. Oomens, Vibrational spectroscopy of bare and solvated ionic complexes of biological relevance, Mass Spectrometry Reviews 28 (2009) 468–494.
[27] T.D. Fridgen, Infrared consequence spectroscopy of gaseous protonated and metal ion cationized complexes, Mass Spectrometry Reviews 28 (2009) 586–607.
[28] J.J. Valle, J.R. Eyler, J. Oomens, D.T. Moore, A.F.G. van der Meer, G. von Helden, G. Meijer, C.L. Hendrickson, A.G. Marshall, G.T. Blakney, Free electron laser-Fourier transform ion cyclotron resonance mass spectrometry facility for obtaining infrared multiphoton dissociation spectra of gaseous ions, Review of Scientific Instruments 76 (2005) 0231031–0231037.
[29] J. Valle Jose, Differentiation of carbohydrate stereoisomers by infrared multiple photon dissociation spectroscopy using a free electron laser and a Fourier transform ion cyclotron resonance mass spectrometer, Ph.D. Thesis, Chemistry, University of Florida, Gainesville, 2005, p. 172.
[30] N.C. Polfer, J.J. Valle, D.T. Moore, J. Oomens, J.R. Eyler, B. Bendiak, Differentiation of isomers by wavelength-tunable infrared multiple photon dissociation-mass spectrometry: application to glucose-containing disaccharides, Analytical Chemistry 78 (2006) 670–679.
[31] S.E. Stefan, J.R. Eyler, Differentiation of methyl-glucopyranoside anomers by infrared multiple photon dissociation with a tunable $CO_2$ laser, Analytical Chemistry 81 (2009) 1224–1227.
[32] S.E. Stefan, J.R. Eyler, Differentiation of glucose-containing disaccharides by infrared multiple photon dissociation with a tunable $CO_2$ laser and Fourier transform ion cyclotron resonance mass spectrometry, International Journal of Mass Spectrometry 297 (2010) 96–101.
[33] E.B. Cagmat, J. Szczepanski, W.L. Pearson, D.H. Powell, J.R. Eyler, N.C. Polfer, Vibrational signatures of metal-chelated monosaccharide epimers: gas-phase infrared spectroscopy of $Rb^+$-tagged glucuronic and iduronic acid, Physical Chemistry Chemical Physics 12 (2010) 3474–3479.
[34] S.E. Stefan, M. Ehsan, W.L. Pearson, A. Aksenov, V. Boginski, B. Bendiak, J.R. Eyler, Differentiation of closely related isomers: application of data mining techniques in conjunction with variable wavelength infrared multiple photon dissociation mass spectrometry for identification of glucose-containing disaccharide ions, Analytical Chemistry 83 (2011) 8468–8476.
[35] D.J. Brown, S.E. Stefan, G. Berden, J.D. Steill, J. Oomens, J.R. Eyler, B. Bendiak, Direct evidence for the ring opening of monosaccharide anions in the gas phase: photodissociation of aldohexoses and aldohexoses derived from disaccharides using variable-wavelength infrared irradiation in the carbonyl stretch region, Carbohydrate Research 346 (2011) 2469–2481.
[36] F. Franks, J.R. Hall, D.E. Irish, K. Norris, The effect of cations on the anomeric equilibrium of D-glucose in aqueous solutions – a Raman-spectral study, Carbohydrate Research 157 (1986) 53–64.
[37] S.J. Angyal, Complexes of metal cations with carbohydrates in solution, Advances in Carbohydrate Chemistry and Biochemistry 47 (1989) 1–43.
[38] P. Dais, Carbon-13 nuclear magnetic relaxation and motional behavior of carbohydrate molecules in solution, Advances in Carbohydrate Chemistry and Biochemistry 51 (1995) 63–131.
[39] K. Gessler, N. Krauss, T. Steiner, C. Betzel, A. Sarko, W. Saenger, β-D-cellotetraose hemihydrate as a structural model for cellulose II. An X-ray diffraction study, Journal of the American Chemical Society 117 (1995) 11397–11406.
[40] B.A. Cerda, C. Wesdemiotis, Thermochemistry and structures of $Na^+$ coordinated mono- and disaccharide stereoisomers, International Journal of Mass Spectrometry 189 (1999) 189–204.
[41] G.A. Jeffrey, M. Sundaralingam, Bibliography of crystal structures of carbohydrates, nucleosides, and nucleotides for 1979 and 1980; addenda and errata from 1970 to 1978; and index for 1935–1980, Advances in Carbohydrate Chemistry and Biochemistry 43 (1985) 203–421.
[42] S. Honda, K. Yamamoto, S. Suzuki, M. Ueda, K. Kakehi, High-performance capillary zone electrophoresis of carbohydrates in the presence of alkaline earth metal ions, Journal of Chromatography 588 (1991) 327–333.
[43] S. Honda, Separation of neutral carbohydrates by capillary electrophoresis, Journal of Chromatography A 720 (1996) 337–351.
[44] S. Perez, Molecular modeling in glycoscience, in: Comprehensive Glycoscience – From Chemistry to Systems Biology, Elsevier, Amsterdam, 2007, pp. 347–388.
[45] A. Varki, Glycan-based interactions involving vertebrate sialic-acid-recognizing proteins, Nature 446 (2007) 1023–1029.
[46] Y. Kajihara, Y. Tanabe, S. Sasaoka, R. Okamoto, Homogeneous human complex-type oligosaccharides in correctly folded intact glycoproteins: evaluation of oligosaccharide influence on protein folding, stability, and conformational properties, Chemistry – A European Journal 18 (2012) 5944–5953, S5944/5941–S5944/5925.
[47] Z.R. Zhou, S. Ogden, J.A. Leary, Linkage position determination in oligosaccharides – MS/MS study of lithium-cationized carbohydrates, Journal of Organic Chemistry 55 (1990) 5444–5446.
[48] N.C. Polfer, J. Oomens, D.T. Moore, G. von Helden, G. Meijer, R.C. Dunbar, Infrared spectroscopy of phenylalanine Ag(I) and Zn(II) complexes in the gas phase, Journal of the American Chemical Society 128 (2006) 517–525.
[49] N.C. Polfer, J. Oomens, Reaction products in mass spectrometry elucidated with infrared spectroscopy, Physical Chemistry Chemical Physics 9 (2007) 3804–3817.
[50] A.G. Marshall, T.C.L. Wang, T.L. Ricca, Tailored excitation for Fourier transform ion cyclotron resonance mass spectrometry, Journal of the American Chemical Society 107 (1985) 7893–7897.
[51] S.H. Guan, A.G. Marshall, Stored waveform inverse Fourier transform (SWIFT) ion excitation in trapped-ion mass spectometry: theory and applications, International Journal of Mass Spectrometry and Ion Processes 158 (1996) 5–37.
[52] D. Oepts, A.F.G. Vandermeer, P.W. Vanamersfoort, The free electron laser user facility FELIX, Infrared Physics and Technology 36 (1995) 297–308.
[53] W.D. Cornell, P. Cieplak, C.I. Bayly, I.R. Gould, K.M. Merz, D.M. Ferguson, D.C. Spellmeyer, T. Fox, J.W. Caldwell, P.A. Kollman, A second generation force field for the simulation of proteins, nucleic acids, and organic molecules, Journal of the American Chemical Society 117 (1995) 5179–5197.
[54] P. Hohenberg, W. Kohn, Inhomogeneous electron gas, Physical Review 136 (1964) B864–B871.
[55] W. Kohn, L.J. Sham, Self-consistent equations including exchange and correlation effects, Physical Review 140 (1965) A1133–A1138.
[56] C. Lee, W. Yang, R.G. Parr, Development of the Colle–Salvetti correlation-energy formula into a functional of the electron density, Physical Review B 37 (1988) 785–789.
[57] HyperChem(™) Professional 7.51, Hypercube, Inc., Gainesville, FL, 2007.
[58] F. Zuccarello, G. Buemi, A theoretical study of D-glucose, D-galactose, and parent molecules: solvent effect on conformational stabilities and rotational motions of exocyclic groups, Carbohydrate Research 273 (1995) 129–145.

[59] F. Momany, M. Appell, J. Willett, U. Schnupf, W. Bosma, DFT study of α-and β-D-galactopyranose at the B3LYP/6-311++ G** level of theory, Carbohydrate Research 341 (2006) 525–537.
[60] F. Momany, M. Appell, J. Willett, W. Bosma, B3LYP/6-311++ G** geometry-optimization study of pentahydrates of α- and β-D-glucopyranose, Carbohydrate Research 340 (2005) 1638–1655.
[61] G. Chang, W.C. Guida, W.C. Still, An internal-coordinate Monte Carlo method for searching conformational space, Journal of the American Chemical Society 111 (1989) 4379–4386.
[62] M.J. Frisch, G.W. Trucks, H.B. Schlegel, G.E. Scuseria, M.A. Robb, J.R. Cheeseman, J.A. Montgomery Jr., T. Vreven, K.L.N. Kudin, J.C. Burant, J.M. Millam, S.S. Iyengar, J. Tomasi, V. Barone, B. Mennucci, M. Cossi, G. Scalmani, N. Rega, G.A. Petersson, H. Nakatsuji, M. Hada, M. Ehara, K. Toyota, R. Fukuda, J. Hasegawa, M. Ishida, T. Nakajima, Y. Honda, O. Kitao, H. Nakai, M. Klene, X. Li, J.E. Knox, H.P. Hratchian, J.B. Cross, V. Bakken, C. Adamo, J. Jaramillo, R. Gomperts, R.E. Stratmann, O. Yazyev, A.J. Austin, R. Cammi, C. Pomelli, J.W. Ochterski, P.Y. Ayala, K. Morokuma, G.A. Voth, P. Salvador, J.J. Dannenberg, V.G. Zakrzewski, S. Dapprich, A.D. Daniels, M.C. Strain, O. Farkas, D.K. Malick, A.D. Rabuck, K. Raghavachari, J.B. Foresman, J.V. Ortiz, Q. Cui, A.G. Baboul, S. Clifford, J. Cioslowski, B.B. Stefanov, G. Liu, A. Liashenko, P. Piskorz, I. Komaromi, R.L. Martin, D.J. Fox, T. Keith, M.A. Al-Laham, C.Y. Peng, A. Nanayakkara, M. Challacombe, P.M.W. Gill, B. Johnson, W. Chen, M.W. Wong, C. Gonzalez, J.A. Pople, Gaussian 03, Gaussian, Inc., Wallingford CT, 2004.
[63] G.I. Csonka, Proper basis set for quantum mechanical studies of potential energy surfaces of carbohydrates, Journal of Molecular Structure: THEOCHEM 584 (2002) 1–4.
[64] U. Schnupf, J.L. Willett, W.B. Bosma, F.A. Momany, DFT study of α- and β-D-allopyranose at the B3LYP/6-311++G** level of theory, Carbohydrate Research 342 (2007) 196–216.
[65] G.I. Csonka, A.D. French, G.P. Johnson, C.A. Stortz, Evaluation of density functionals and basis sets for carbohydrates, Journal of Chemical Theory and Computation 5 (2009) 679–692.
[66] A.P. Scott, L. Radom, Harmonic vibrational frequencies: an evaluation of Hartree–Fock, Moller–Plesset, quadratic configuration interaction, density functional theory, and semiempirical scale factors, Journal of Physical Chemistry 100 (1996) 16502–16513.
[67] M.P. Andersson, P. Uvdal, New scale factors for harmonic vibrational frequencies using the B3LYP density functional method with the triple-ξ basis set 6-311+G(d,p), Journal of Physical Chemistry A 109 (2005) 2937–2941.
[68] J.P. Merrick, D. Moran, L. Radom, An evaluation of harmonic vibrational frequency scale factors, Journal of Physical Chemistry A 111 (2007) 11683–11700.
[69] P. Tomasik, M. Palasinski, S. Wiejak, The thermal decomposition of carbohydrates. Part I. The decomposition of mono-, di-, and oligosaccharides, Advances in Carbohydrate Chemistry and Biochemistry 47 (1989) 203–278.